Published in final edited form as:
Dev Cell. 2014 June 9; 29(5): 547–561. doi:10.1016/j.devcel.2014.04.021.

Mechanism of Cytokinetic Contractile Ring Constriction in Fission Yeast

Matthew R. Stachowiak[1], **Caroline Laplante**[2], **Harvey F. Chin**[1], **Boris Guirao**[1], **Erdem Karatekin**[3,4], **Thomas D. Pollard**[2,5,6], and **Ben O'Shaughnessy**[1,*]

[1]Department of Chemical Engineering, Columbia University, 116th and Broadway, New York, NY 10027, USA, Yale University, P.O. Box 208103, New Haven, CT 06520, USA

[2]Department of Molecular, Cellular, and Developmental Biology, Yale University, P.O. Box 208103, New Haven, CT 06520, USA

[3]Department of Cellular and Molecular Physiology, School of Medicine, Yale University, P.O. Box 208103, New Haven, CT 06520, USA

[4]Nanobiology Institute, Yale University, P.O. Box 208103, New Haven, CT 06520, USA

[5]Department of Molecular Biophysics and Biochemistry, Yale University, P.O. Box 208103, New Haven, CT 06520, USA

[6]Department of Cell Biology, Yale University, P.O. Box 208103, New Haven, CT 06520, USA

SUMMARY

Cytokinesis involves constriction of a contractile actomyosin ring. The mechanisms generating ring tension and setting the constriction rate remain unknown, since the organization of the ring is poorly characterized, its tension was rarely measured, and constriction is coupled to other processes. To isolate ring mechanisms we studied fission yeast protoplasts, where constriction occurs without the cell wall. Exploiting the absence of cell wall and actin cortex, we measured ring tension and imaged ring organization, which was dynamic and disordered. Computer simulations based on the amounts and biochemical properties of the key proteins showed that they spontaneously self-organize into a tension-generating bundle. Together with rapid component turnover, the self-organization mechanism continuously reassembles and remodels the constricting ring. Ring constriction depended on cell shape, revealing that the ring operates close to conditions of isometric tension. Thus, the fission yeast ring sets its own tension, but other processes set the constriction rate.

*Contact: bo8@columbia.edu.

INTRODUCTION

Cytokinesis in animal, fungal and amoeboid cells involves constriction of an actomyosin contractile ring, thought to develop tension due to interactions of myosin-II motor proteins (Fujiwara and Pollard, 1976; Mabuchi and Okuno, 1977) with actin filaments (Schroeder, 1972). The proteins of the ring are widely conserved and particularly well characterized in the fission yeast *Schizosaccharomyces pombe*, where more than 130 genes are known to participate (Pollard and Wu, 2010) and the amounts of many proteins were measured in the ring (Wu and Pollard, 2005). However, since the spatial organization and motions of these components within the ring are poorly characterized, and the ring tension has not been measured, the mechanism that generates tension is unknown. Neither is the mechanism that sets the rate of ring constriction established, as constriction in *S. pombe* is coupled to septation, the poorly understood process of cell wall deposition in the wake of the constricting ring (Sipiczki and Bozsik, 2000). Analogous situations hold in other organisms: mathematical models variously proposed that constriction is coupled to cortical tension, cytoplasmic viscosity and cell elasticity (Biron et al., 2005; Zhang and Robinson, 2005).

Direct evidence that cytokinetic rings generate tension comes from studies of echinoderm embryos (Rappaport, 1967, 1977), but the ring organization responsible for the measured tensions of ~8–15 nN is unknown. Similar to striated muscle, the ring could have an ordered architecture based on sarcomere-like repeat units (Carvalho et al., 2009; Schroeder, 1975). However, neither fluorescence nor electron micrographs of constricting fission yeast rings indicated highly ordered sarcomeres (Bezanilla et al., 2000; Kamasaki et al., 2007; Kanbe et al., 1989; Pelham and Chang, 2002).

The organization of the ring could be static, with components rigidly anchored to the membrane, or components could be mobile within a more dynamic organization. Component motions have not been measured, and the identity and mobility of anchors attaching the ring to the membrane are unknown. Formin Cdc12p associates processively with actin filament barbed ends (Kovar et al., 2006) and may be anchored to the membrane as in nodes, the precursor protein complexes of the ring (Laporte et al., 2012; Vavylonis et al., 2008). Myosin-II may be anchored independently, as it remains at the division site after disassembly of actin filaments in fission yeast (Naqvi et al., 1999) and animal cells (Schroeder and Otto, 1988).

During constriction contractile rings shed material without loss of function, but the mechanism is unclear. In animal cells the ring volume decreases during constriction (Schroeder, 1972), and in fission yeast the amounts of actin-binding proteins α-actinin Ain1p, F-BAR Cdc15p and IQGAP Rng2p decrease in proportion to ring length (Wu and Pollard, 2005), suggesting the same is true of actin. On short timescales ring components turn over, including myosin-II and formin Cdc12p, both in ~30 s (Pelham and Chang, 2002; Yonetani et al., 2008). Actin presumably also turns over, as the actin monomer sequestering agent latrunculin A disassembles contractile rings in ~1 min.

Here we used fission yeast protoplasts (Jochova et al., 1991; Mishra et al., 2012) to isolate the mechanism of ring constriction from septation. As yeast protoplasts lack a cell wall and

actin cortex, we could measure contractile ring tension from furrowing of the membrane and image the ring organization, which was dynamic and disordered. Detailed computer simulations showed that components stochastically self-organize into a ring with a tightly bundled architecture whose tension was close to the measured value. Self-organization amplifies the tension by orienting tense filaments and increasing the number of actin-myosin interactions, and remodels the constricting ring by continuous reassembly of components that rapidly turn over. We compressed protoplasts to study the effect of cell shape on ring constriction, which occurs by sliding along the membrane without septation. This revealed that thering operates close to conditions of isometric tension. Thus, the *S. pombe* contractile ring sets its own tension, but the rate of constriction is set by other processes, possibly influenced by the ring's tension.

RESULTS

Fission yeast protoplasts form nodes and assemble contractile rings

We prepared protoplasts of fission yeast cells by treatment with enzymes to digest the cell wall. Protoplasts lost their polarity (Fig. S1A,B) and adopted a rounded shape (Fig. 1A,B), with an equatorial circumference of L_{proto} = 18.1 ± 1.9 μm (mean ± SD, n = 18), almost twice that of intact cells (~11 μm). Maintaining the digesting enzymes in the medium during imaging prevented cell wall regrowth that could interfere with ring constriction and our measurements of membrane tension (see below). This was confirmed by the rounded cell shapes (>95% of protoplasts). In a previous study of ring constriction in protoplasts, the enzymes were removed and the cells assumed a variety of irregular shapes (Mishra et al., 2012).

We tracked contractile ring assembly in protoplasts with the myosin-II regulatory light chain fused to three molecules of GFP (Rlc1p-3GFP). Contractile rings formed from cortical puncta containing myosin-II that were indistinguishable from cytokinesis nodes except for being distributed over the entire cortex and condensing into strands (Fig. 1C). As in intact cells (Vavylonis et al., 2008) we observed two distinct populations: nodes undergoing apparently diffusive motion; and nodes making stochastic, directed, stop-go motions. A Bayesian analysis (Monnier et al., 2012) of the first population confirmed unconstrained2D diffusion in the plane of the plasma membrane (probability > 0.99), with a linear time dependence for theaverage mean squared displacement, MSD(t) = MSD(0) + 4Dt (Fig. 1D, Fig. S1C–E, and Movie S1) (n = 64 nodes, 15 cells). The diffusion constant, D, was 31.2 nm^2/s, giving a node drag coefficient γ_{node} of 130 pN·s/μm from the Einstein relation $\gamma_{node} = k_BT/D$. This is a lower bound, as sources other than thermal motion may contribute to the diffusion. Nodes undergoing directed motion had a mean velocity v_{node} = 30.9 ± 27.2 nm/s in bursts lasting ~22 s (mean ± SD, n = 54 nodes, 13 cells, Fig. 1E, Fig. S1F, and Movie S2), so the mean force acting on the node was $\gamma_{node}v_{node} \approx 4$ pN. Thus, in protoplasts the node drag coefficient, velocity, duration of motion and force all lie within ~33% of the values in intact cells (Vavylonis et al., 2008).

In intact cells stop-go motions condense nodes directly into a contractile ring (Vavylonis et al., 2008), whereas protoplasts assembled rings unreliably by a variety of pathways: by coalescence of separate short strands of nodes, emergence of long strands of nodes from

clusters of Rlc1p-3GFP or from strands of nodes growing from disassembling rings (Fig. 1F) (n = 2 cells each).

Protoplast rings constrict without septation in a myosin-dependent manner

In intact cells, the constricting ring lies at the leading edge of a septum growing between the daughter cells. By contrast, protoplasts did not form septa nor cleave, and rings that contained both myosin-II and actin filaments constricted while sliding against the plasma membrane (Fig. 1G,H and Movie S3) as previously observed (Mishra et al., 2012). The constriction rate in protoplasts (change of ring circumference with time) increased over time, with a mean time-averaged value of 0.23 ± 0.08 μm/min (mean ± SD, n = 18), similar in magnitude to the rate in intact cells, 0.34 ±0.06 μm/min (n = 20, Fig. 1I). In protoplasts with the temperature-sensitive *myo2-E1* mutation that lowers the affinity of Myo2p for actin filaments (Lord and Pollard, 2004), the mean constriction rate was lower, 0.08 μm/min (n = 3, Fig. 1I), showing that ring constriction depends on myosin-II. The concentration of myosin-II in rings increased as they shortened, although the total amount declined, similar to intact cells (Wu and Pollard, 2005), with an almost identical rate of loss (8.3 % versus 8.6% myosin loss per 10% ring shortening) (Fig. S1G,H).

Contractile rings generate ~390 pN of tension

Tension production is thought to be a principal function of the ring, but this most basic mechanical property has been measured in only a few instances, in large fertilized echinoderm eggs (Rappaport, 1967, 1977).

We exploited the properties of protoplasts to measure ring tension. Sliding contractile rings furrowed the membrane of spherically shaped protoplasts (Fig. 2A), and since fission yeast cells lack an actin cortex we assumed that the force resisting this furrowing derives purely from the plasma membrane tension, σ. Thus, by measuring σ, we could deduce the ring tension from a simple force balance. We used micropipette aspiration, measuring the suction pressure ΔP necessary to aspirate a tongue of length l equal to the pipette radius R_p (Fig. 2B) (Evans and Yeung, 1989). This gave a value σ = 0.28 ± 0.28 mN/m (mean ± SD, n = 9). From the furrow shape we then determined the component of σ acting in the plane of the ring of radius R_{ring} and balanced this with the centripetal force per unit length due to ring tension, T/R_{ring}(Fig. 2A and Extended Experimental Procedures). Assuming the measured membrane tension to be the mean of the values in the two lobes of protoplasts with constricting rings, this yielded a ring tension of 391 ± 154 pN (n = 12).

Myosin-II and formin Cdc12p are mobile in constricting rings, and formins move more rapidly

We tracked the motions of fluorescently tagged formin Cdc12p and myosin-II in constricting rings at high spatial and temporal resolution. Protoplasts are favorable for these observations because we could image 2.5–14 μm of a ring in mildly compressed protoplasts within a single confocal plane (Fig. 2C). Imaging long spans of rings in intact cells normally requires reconstructions of Z-sections, with lower resolution along the Z-axis. Kymographs showed that fluorescent spots containing each protein moved bidirectionally around the ring during constriction (Fig. S2A–D). The speed distribution of Cdc12p spots appeared bimodal,

suggesting heterogeneity in anchoring, but for simplicity we assumed uniform anchoring of Cdc12p in this analysis. The mean speed of all Cdc12p spots (20.2 ± 27.5 nm/s) was ~6.5-fold greater than that of myosin-II spots (3.1 ± 4.7 nm/s) (Fig. 2D–G and Movies S4 and S5). Thus a substantial fraction of formin spots moved independently of myosin-II. For example, 43% of the formin spots, with speeds >10 nm/s, moved faster than 90% of the myosin-II spots.

Formin dimers are organized randomly in the contractile ring

Profiles of formin Cdc12p fluorescence intensity along rings in compressed cells (Fig. 2H,I) displayed no spatial correlations (Fig. 2J), consistent with a random distribution. To test for clustering, we simulated fluorescence intensity distributions produced by randomly positioned clusters, assuming a constant overall formin density of 15 dimers/μm, as previously measured (Wu and Pollard, 2005) (Fig. S2E). Comparing the simulated intensity fluctuation about the mean with the measured value, clusters containing only one formin dimer gave the best fit (Fig. S2F,G), suggesting that individual formin dimers are distributed randomly around the contractile ring.

Model of the contractile ring in protoplasts

We developed a stochastic computer simulation of the ring that explicitly models the key molecular components (Fig. 3) to answer several major questions: How are the principal ring components organized to generate tension? How much tension do rings generate? How is the organization achieved? How does the ring remodel as it constricts, while preserving its organization and tension? The simulation is based on measurements from this and previous studies that constrain the amounts of each component and their biochemical mechanisms, the spatial distributions, motions and turnover rates of components, and the model parameters (Table S1). Here we describe the main features of the model, with additional detail in Extended Experimental Procedures.

Our simulations approximated the ring as a quasi-2D structure parallel to the plasma membrane, based on our experiments showing that rings are <0.4 μm thick perpendicular to the membrane (Fig. 1J and S3A,B), significantly less than the mean actin filament length (~1.3 μm, see below). Moreover, a previous study estimated that actin filaments make a small ~8° angle with the membrane during ring assembly (Laporte et al., 2011).

Consistent with our measurements (Fig. 2D–G), the model used laterally mobile myosin-II clusters and formin Cdc12p dimers independently anchored to the inside of the plasma membrane (Fig. 3B). The myosin-II clusters were assumed to comprise ~40 molecules as in the precursor nodes, but we did not specify their internal organization, which is unknown. Formin and myosin turned over in the ring (Fig. 3A), with spatially random binding rates in a zone 0.2 μm wide, as this choice produced a steady state with formins randomly distributed along the ring (Fig. S3E) and the components extending ~0.2 μm across the ring (Fig. 4F below), in agreement with present and previous experiments (Fig. 2H–J) (Kanbe et al., 1989; Wu and Pollard, 2005).

Upon binding to the ring, formin dimers nucleate and polymerize randomly oriented actin filaments (Fig. 3A). A filament is captured and drawn toward a myosin-II cluster if it grows

to within itsca pture radius, r_{myo} = 0.1 μm (Fig. 3B and Table S1). Following such a binding event, myosin pulls on the filament (Fig. 3B) with a force f_{myo} = 4 pN, inferred from our measurements of node motions in protoplasts, creating tension in the filament. Note that the assumed anchoring of formins to the membrane, and the production of tension by myosin-II pulling on actin filaments against these anchors, is realized in the precursor nodes that assemble to form the ring (Vavylonis et al., 2008). The maximum force a cluster could exert was assumed to be 40 pN, given the 40 available myosin heads (Extended Experimental Procedures). Subsequent interactions with nearby myosin-II clusters tend to rotate and bundle filaments (Fig. 3C). Dynamic α-actinin crosslinks, represented as springs, connect nearby actin filaments (Fig 3B) (Laporte et al., 2012). An actin filament exits the ring when the formin anchoring its barbed end unbinds from the ring, as formin Cdc12p binds barbed ends with high affinity (residence time >1000 s in vitro (Kovar et al., 2006)). Throughout, filaments stochastically shorten due to cofilin-mediated severing; distal segments of severed filaments dissociate from the ring (Fig. 3A) (Michelot et al., 2007). The actin filaments are semi-flexible, with persistence length l_p = 10 μm (Table S1).

The principal outputs of the simulation are ring organization and tension. Stochastic sequences of binding, nucleation, growth, capture, rotation, bundling and unbinding occurred throughout the ring and spontaneously organized the components into a tension-producing bundle.

Results of simulations and comparisons with experiment

Determination of unknown parameters from simulation results—The myosin-II, formin, and α-actinin binding and unbinding rates were tuned so that the component densities and turnover rates matched experimental values (Table S1) and our own measurements of myosin concentration (Fig. S1H). The actin filament polymerization and severing rates were tuned so the total amount of actin, and the time for ring disintegration after shutdown of actin polymerization, matched measured or estimated values in fission yeast (Fig S3D and Table S1).

We determined the anchor drag coefficients for formin, γ_{for}= 1.9 nN·s/μm, and for myosin, γ_{myo} = 1.3 nN·s/μm,by tuning them until the simulated mean velocity of each component matched the values we observed in live protoplasts. Kymographs of formin and myosin motions were then qualitatively similar in protoplasts (Fig. 2D,F) and ring simulations (Fig. 2K,L).

The ring self-organizes into a dynamic, tension-producing disordered bundle —Remarkably, actin filaments and myosin-II clusters in the simulation spontaneously self-organized into a bundled ring that produced tension (Fig. 4 and Movie S6). The bundled organization was disordered, with formins and myosin-II clusters randomly positioned along the ring and actin filaments having random orientations primarily parallel or antiparallel to the ring (Figs. S3E and 4L). The organization was dynamic, due to the continuous throughput of components that entered the ring, self-organized and then dissociated.

Three mutually reinforcing mechanisms drove the self-organization process. First, actin filaments growing in random directions from formins were aligned with the ring by

interactions with myosin clusters, a zippering process in which binding to one myosin cluster rotated the filament to within the capture radius of the next (Fig. 4C). Filaments nucleated orthogonally to the ring were less likely to be captured and bundled, and contributed little to ring tension. Second, tension produced by myosin clusters that captured two or more actin filaments moved the myosin so as to align the filaments (Fig. 4D). Third, by binding to the aligned actin filaments myosin clusters condensed into a long ribbon ~0.1 μm wide (Fig. 4E,F), similar to the diameter of the ring in electron micrographs (Kanbe et al., 1989).

Tension in simulated rings agrees with the experimental value measured in protoplasts—The simulated contractile ring generated 340 ± 57 pN of tension at the onset of constriction (Fig. 4A), close to the value we measured in protoplasts, 390 ± 154 pN. As constriction proceeded, tension increased to ~630 ± 80 pN after the ring shortened by 80% (Fig 4B), due to the increasing concentration of myosin-II. Due to the dynamic nature of the ring organization, the simulated tension fluctuated about its mean value over ~29 s, similar to the actin turnover time (Fig. 4A).

Relationship between organization and tension in the ring—The mechanism producing tension in individual actin filaments was the formin-mediated anchoring of filament barbed ends, ensuring that pointed ends grew toward myosin-II clusters correctly oriented for tension-producing interactions (Fig. 3B). Self-organization into a bundle boosted the filament tensions by increasing the number of myosin clusters binding a filament, and maximized their contributions to ring tension by orienting them parallel to the ring (Fig. 4).

To quantify these mechanisms, a calculation showed that the mean ring tension T obeys the approximate relation $T \approx f_{\mathrm{myo}}\, c_{\mathrm{fil}} \langle l \rangle\, \Psi_{\mathrm{bund}} \Psi_{\mathrm{sarc}}$, featuring two statistical properties of the ring organization: the bundling coefficient $\Psi_{\mathrm{bund}} = \langle \cos^2\theta \rangle$; and the "sarcomericity" $\Psi_{\mathrm{sarc}} = \langle \int_0^l ds\, c_{\mathrm{myo}}(s)\, s \rangle / \langle l \rangle$ (Extended Experimental Procedures). Here angular brackets denote averaging, θ is the angle an actin filament tangent makes with the ring circumferential direction (Fig. 4G), c_{fil} is the mean density of actin filaments per length of ring, and $c_{\mathrm{myo}}(s)$ the density of engaged myosin clusters a distance s from the barbed end along a filament of length l. Ψ_{bund} measures the orientation of filaments parallel to the ring, and Ψ_{sarc} the mean number of myosin clusters bound to a filament, weighted by their distances from the barbed end (Fig. 4G and H). The sarcomericity factor reflects the fact that a myosin cluster produces tension only in the actin filament segment between its binding site and the anchored barbed end. Hence, the more distant the binding site from the barbed end, the greater the length of actin filament affected and the contribution to ring tension. The sarcomericity and tension are greater with more interactions, and are maximized in a sarcomeric organization where myosin binds near the pointed ends of actin filaments (Huxley, 1974).

Myosin II was essential for organizing actin filaments into a tension-generating bundle (Fig. 4I–O). In "wild-type" simulations, Ψ_{bund} =0.8, close to perfect alignment (Ψ_{bund} = 1), and Ψ_{sarc} = 4.2 (Movie S6). When we allowed myosin to exert normal pulling forces but not to

capture and rotate filaments (Myo2Δcapture), bundling failed, $\Psi_{bund} = 0.42$, the sarcomericity decreased to $\Psi_{sarc} = 0.2$ and tension was reduced by 97% (Fig. 4I–K,M).

By contrast α-actinin, the most abundant passive crosslinker in the ring, contributed little to bundling and tension. Its absence had only a small effect on the simulations (Fig. 4I–K,O), consistent with the lack of cytokinesis defects in cells without α-actinin (Wu et al., 2001). Without myosin, α-actinin crosslinks did not form rings and caused filaments that grew toward one another to splay sideways into orthogonal bundles ($\Psi_{bund} \approx 0.41$, Fig. 4I–K,N).

Tension and organization of the simulated ring are robust to parameter variations—The ability of our simulations to form rings and produce tension was robust in a range about the wild type parameter values of Table S1 (Fig. 5 and Extended Experimental Procedures). Spontaneous generation of functional rings with bundled organization and tension close to the experimental value required that the components bind in a zone $\lesssim 0.4$ μm wide, that formins have an anchor mobility $\lesssim 2$ μm/nN·s and that myosin clusters have a capture radius $\gtrsim 70$ nm and an anchor mobility $\gtrsim 0.2$ μm/nN·s (Fig. 5A –F). Greater myosin anchor mobility promoted self-organization by enlarging the effective radius to capture and zipper actin filaments into bundles (Fig. 4C–E). By contrast, increased formin anchor mobility allowed actin filament barbed ends to be pulled toward myosin clusters, lowering the sarcomericity and thus lowering the tension somewhat (Fig. 5D). A favorable outcome for the simulations was insensitive to bias in the orientation of the nucleated actin filaments and the actin filament bending modulus (Fig. 5G,H), and to actin polymerization and severing rates at fixed mean filament length (data not shown).

Ring sliding-constriction in protoplasts: tension works against membrane anchor drag forces—Our principal motivation for using protoplasts was to decouple the ring from other complex systems, including the poorly characterized septation process. We anticipated that, given the absence of cell wall and actin cortex, tension would drive ring sliding-constriction resisted only by simple drag forces from anchors connecting the ring to the membrane.

To test this hypothesis we developed a model of ring sliding-constriction in a protoplast, with uniformly distributed anchors attaching the ring to the membrane (Fig. 3D and Extended Experimental Procedures). The predictions for non-spherically shaped protoplasts are particularly useful, as constricting rings bend out of plane into a sequence of shapes specific to the model. Thus we compressed protoplasts into a family of cheese wheel shapes (Fig. 6A,B), and measured ring shapes as they slid and constricted in these cells (Fig. 6C).

These experiments confirmed several model predictions. First, rings adopted bent shapes, with the central portion of the ring on the flat surface lagging behind the edges (Fig. 6C and Movie S7). The predicted and observed shapes agreed closely in 6 of 7 protoplasts (Fig. S4A). Second, the ring bending increased over time as rings constricted (Fig. 6D and S4B). Third, rings bent to a greater extent in protoplasts that were more flattened (Fig. 6D and S4B).

These are stringent tests of the model with no free parameters, as the predicted sequence of ring shapes depends only on the cell shape, and is *independent* of the values of the ring tension and drag coefficient (Extended Experimental Procedures). Thus, ring tension in protoplasts is opposed only by drag forces against the cell membrane, and the ring is isolated from other systems.

The contractile ring sets its own tension, not the constriction rate—Having verified that the sliding-constriction model (Fig. 3D) correctly describes rings in protoplasts, we could use the model to examine mechanisms of the isolated ring. We measured lengths of constricting rings over time, $L(t)$, and the shapes of the protoplasts containing the rings (Fig. 6B). For each cell shape we used the sliding-constriction model to calculate $L(t)$, using as input data the values of ring tension versus length calculated from our ring simulation (Fig. 4B). The model captured the observed increase in constriction rate with time (Fig. 6E and S4C, model I), using the total anchor drag coefficient γ_{ring} as a fitting parameter (Table S1). The increase is due to cell shape: where the protoplast is steeper, the centripetal force due to tension has a greater component parallel to the surface (Fig. 3D). When we assumed that the anchoring drag is proportional to ring length, the fit was significantly worse (model II, Fig. 6E,F and S4C).

This procedure used isometric tension values, i.e. calculated from simulations of rings of fixed length L. We hypothesized that these tension values remain applicable even when the ring constricts, since constriction is much slower (10–80 min) than the turnover of ring components (<1 min). The agreement with experiment (Fig. 6E) supports this hypothesis. Thus, the ring sets its tension close to the isometric value, but does not set the constriction rate. The latter is determined by the response of the sliding membrane anchors.

We could not fit the experimental constriction profiles with two alternative models, in which constriction rates are self-determined and independent of the load from the anchors (models III and IV, Figs. 6E–F and S4C, and Extended Experimental Procedures). In the first, the ring constricts at a fixed rate proportional to its initial length, as in *C. elegans* embryos (Carvalho et al., 2009). In the second, the constriction rate is proportional to the myosin-II concentration.

Rapid turnover of ring components maintains ring tension and organization—Ring organization and tension depended on turnover of myosin, formin and actin. After running ring simulations to steady state, abruptly switching off the turnover of all components resulted in sliding of formins and aggregation of myosin clusters (Fig. 7A), as well as decay of the sarcomericity and tension (Fig. 7B). Thus, the self-organization of rapidly turning over components continually renews the ring organization, preventing its dissipation and the accompanying loss of tension (Fig. 7D).

Actin in the ring turns over ~3-fold faster than formin—Direct measurement of actin turnover in the ring has not been possible, since fluorescently tagged actin is not incorporated into the fission yeast contractile ring (Chen et al., 2012; Wu and Pollard, 2005). Simulations and exact calculations (see Supplemental Experimental Procedures) of a FRAP assay predicted an actin recovery half time of 11 s (Fig. 7C), ~3-fold faster than that of

formin Cdc12p (30 s, Yonetani et al., 2008) (see Fig. 7C for comparison). This rapid recovery of actin relative to formin is caused by two factors. First, compared to formin actin has an additional route of exit from the ring (severing). By quantitatively tracking how actin exits the simulated ring we determined that 44% of actin turned over with dissociating formins, while the remaining 56% turned over via cofilin-mediated severing. Second, newly polymerized monomers at filament barbed ends are less likely to exit the ring with a severed filament segment than are other monomers positioned closer to the pointed end. Thus, the FRAP recovery curve increases rapidly because initially most of the actin leaving the ring is bleached.

To test the model's assumed turnover mechanisms, we showed that simulations with slower actin polymerization replicated experiments in fission yeast cells expressing mutated formin with reduced polymerization activity (Supplemental Experimental Procedures and Fig. S3C,D).

DISCUSSION

The fission yeast protoplast is a model system to study contractile ring constriction

To isolate the mechanisms of the ring in fission yeast, we studied protoplasts, in which rings constricted by sliding on the plasma membrane without septation (Fig. 1G). While only a small fraction of protoplasts assembled rings (<1%), the rings closely resembled rings in intact cells in terms of node velocities and drag coefficients (Fig. 1D,E), myosin-II concentration profiles and constriction rates (Figs. 1I and S1). Moreover, protoplast rings appear to recruit unconventional myosin-II (Myp2p) and β-glucan synthase (Bgs1p) (Mishra et al., 2013), proteins that join the rings of intact cells late during their maturation, further evidence that protoplast rings are representative of fully formed contractile rings.

The lack of cell wall and actin cortex in fission yeast protoplasts allowed us to measure the tension of the ring (Fig. 2A,B), image ring component motions and spatial organization (Fig. 2C–J) and measure the effect of cell shape on constricting rings (Fig. 6), which showed that the ring sets its tension but not the constriction rate. In summary, protoplasts allowed us to interrogate ring constriction mechanisms quantitatively in a way not presently possible with intact yeast cells.

Ring tension is far smaller in fission yeast than in animal cells, but the stress is similar

The contractile ring tension we measured in protoplasts (~390 pN, Fig. 2A,B) and in simulations (~340 pN, Fig. 4A) is much smaller than the 8,000–15,000 pN measured in large, fertilized echinoderm eggs (Rappaport, 1967, 1977), where constriction is also much faster (~6 min in cells ~100 μm in diameter (Schroeder, 1972)). However, when corrected for cross sectional area of the ring (~0.027 μm^2 in yeast, Wu and Pollard, 2005), the tensions give similar stresses in fission yeast, ~14.5 $nN/\mu m^2$, and echinoderm eggs, 5–10 $nN/\mu m^2$ (Rappaport, 1967, 1977).

Organization of the fission yeast contractile ring is dynamic and disordered

Our experiments revealed a dynamic ring with significant disorder: formins are randomly distributed spatially, most formins move independently of myosin-II, and both components move stochastically with broad bidirectional velocity distributions (Figs. 2 and S2). These features differ from those of an ordered organization of structurally identical contractile units arranged in series, as proposed for *C. elegans* (Carvalho et al., 2009).

Tension production by the ring depends on barbed-end anchoring and self-organization

The mechanisms of actomyosin contractility and tension remain debated. A theoretical bundle of randomly organized actin filaments crosslinked by myosin and α-actinin is not contractile, as myosin-generated pulling (tensile) and pushing (compressive) forces balance. Proposals to resolve this paradox include filament buckling, actin depolymerization effects and end-tracking crosslinkers (Lenz et al., 2012; Mendes Pinto et al., 2012; Zumdieck et al., 2007).

Our results suggest that nature adopts a simple solution in the constricting *S. pombe* ring: the formin-mediated anchoring of actin filament barbed ends to the plasma membrane. This ensures that myosin captures filaments with pointed ends correctly oriented to generate tension (Fig. 3B), similar to the mechanism that draws a broad band of nodes together into a ring (Vavylonis et al., 2008). Ring tension was generated in our simulations by a self-organization process in which actin filaments, made tense in this fashion, self-organized with myosin-II clusters into a tight bundle.

The self-organized bundle is disordered, but its anchoring and organizational statistics are biased for tension (Fig. 4 and Movie S6). We showed the ring tension depends on two organizational properties, the bundling coefficient, Ψ_{bund}, and the sarcomericity, Ψ_{sarc}. The sarcomericity closely tracked tension when parameter values were varied (Fig. 5) and when turnover was shut down (Fig. 7B). The self-assembled bundle has large values of Ψ_{bund} and Ψ_{sarc} since the actin filaments are oriented, the bundle is dense with many myosin clusters binding each filament and barbed end anchoring maximizes the separations between myosin interaction sites and the anchors (Fig. 4H). It will be of interest to measure Ψ_{bund} and Ψ_{sarc} experimentally, possibly by electron or super-resolution fluorescence microscopy.

Consistent with this mechanism of tension production, our experiments showed that formins moved more rapidly around the ring than myosin-II clusters, similar to observations in budding yeast (Wloka et al., 2013). This behavior follows immediately from barbed end anchoring, as actin filaments are always pulled toward their pointed ends regardless of how many myosin clusters they intersect, whereas myosin clusters typically bind many actin filaments with varied orientations and so are pulled in opposing directions, with much lower net speed.

Role of anchor mobility in the production of ring tension

Our simulations showed that weak anchoring of myosin-II promotes the tension-amplifying self-organization processes, since migration of myosin to the midline of the ring and the capturing, aligning and bundling of actin filaments all relied on high myosin mobility (Fig.

4C–E). Consistent with the experimentally measured mean formin speed of ~20 nm/s (Fig. 2E), only ~5% of the load-free velocity of fission yeast Myo2p (Lord and Pollard, 2004), we assumed that the force exerted by myosin-II is not reduced by filament motion, due to the firm anchoring of formin Cdc12p.

Using the best fit anchor drag coefficients from our simulations together with the densities of each component (Table S1), the total drag coefficient from all formin and myosin-II anchors in a 20 μm ring is ~750 nN·s/μm, ~55 times the combined value for all precursor nodes in intact cells (Vavylonis et al., 2008). This suggests that anchoring to the membrane is heavily reinforced following ring assembly. Fitting our sliding-constriction model to constriction profiles in protoplasts gave a total ring drag coefficient 3 – 4 times greater, $\gamma_{ring} \approx 2800 \pm 50$ nN·s/μm. The additional drag could reflect restricted diffusion of membrane lipids through tightly condensed ring anchors as the ring slides, or drag from membrane proteins accumulating ahead of the sliding ring.

Continuous reassembly maintains tension and remodels the ring during constriction

Our simulations describe a ring that reassembles itself every ~30 s, due to the rapid turnover of components that continuously self-organize on arrival in the ring. This prevents decay of the sarcomericity and tension that accompanies displacement of actin filament barbed ends due to myosin-II forces (Fig. 5D and 7D), since barbed ends with mean speed ~20 nm/s (Fig. 2E) translate only ~0.6 μm in the turnover time, about half the mean filament length. When reassembly was blocked in simulations without turnover, the organization decayed to a state of low sarcomericity and tension, with clumped myosin (Fig. 7A,B).

On much longer constriction time scales (~30 min, Fig. 6E), continuous reassembly is the mechanism that remodels the ring: as the ring constricts, it rapidly reassembles at each progressively smaller length (Fig. 7D). The number of binding sites for myosin-II and formins declines, so the number of filaments decreases in proportion to ring length, consistent with the observed decrease in number of formins during constriction (Wu and Pollard, 2005). Thus the actin density is maintained constant, consistent with previous reports of constant density of actin binding proteins (Wu and Pollard, 2005). This mechanism could apply to other species, provided component turnover is faster than constriction.

Role of the contractile ring

The contractile ring presumably has its own tension-velocity relation, the rate of shortening versus tension or external load. The relation is well known for muscle, where tension decreases from its isometric value at zero shortening rate down to zero at the maximum shortening velocity (Huxley, 1974). The relation for the contractile ring, and where on this relation the ring operates, have not been accessible as constriction is coupled to other processes.

Fission yeast protoplasts allowed us to examine these issues in a quantitatively defined situation where the load was supplied by membrane anchor drag forces alone. The constriction data was best fit by a model where the ring operated close to the isometric tension limit. The constriction rate depended on cell shape, far from the zero load limit

where the rate would be independent of external factors and attain its maximum value, a value intrinsic to the ring. Consistent with this, yeast protoplast rings that partially detached from the membrane constricted ~25-fold faster, presumably under nearly zero load (Mishra et al., 2013). Thus, in protoplasts the ring sets its own tension, but does not set the constriction rate.

It follows that the same is true in intact *S. pombe* cells, since rings constrict at a similar rate (Fig. 1I) and thus operate at a similar location on the tension-velocity curve, close to the isometric tension limit. Thus, other processes set the constriction rate; a likely candidate is deposition of the septum that grows centripetally behind the constricting ring. The ring tension might regulate septation to maintain the septum boundary smooth and circular throughout the growth process.

EXPERIMENTAL PROCEDURES

Strains and protoplast preparation

Strains are in Table S2. *S. pombe* cells were grown to OD_{595} of 0.2, and 8–10 mL of cells were harvested in tabletop Beckman centrifuge for 5 min at 2000 rpm. The pellet was resuspended in 2.5 mg/mL each of Lytic (MP Biomedicals) and Lysis (Sigma-Aldrich) enzymes, dissolved in either E-buffer (50 mM sodium citrate, 100 mM phosphate buffer pH 6.0 with 0.6 M sorbitol) or EMM5S yeast minimal medium and incubated for 1 h at 30°C. The resulting protoplasts were washed twice with E-buffer and 0.6 M sorbitol. The protoplast pellet was resuspended in 50 μL mounting medium (50% EMM5S in E buffer with 100 μl NPG 10X, 2.5 mg/mL each of Lytic and Lysis enzyme, and 0.6 or 1.2 M sorbitol), mounted on a glass slide, covered with a coverslip, sealed with VALAP and immediately imaged. Cells expressing GFP-CHD were cultured in YE5S for 24–36 h, then transferred to EMM5S for 24 h before imaging. Protoplasts were compressed by capillary forces pulling the coverslip and slide together.

Microscopy

All imaging used an Olympus IX-71 inverted microscope. Epifluorescence and DIC microscopy used a 60× 1.4 NA Plan-apo objective, appropriate filter sets (DIC, FITC, and RFP), and a Hamamatsu Orca-ER cooled CCD camera (Bridgewater, NJ). Confocal microscopy used either a CSU X-1 spinning disk confocal unit (Yokogawa) and an IXon DU-897 EMCCD camera (Andor) or an Ultraview spinning disk confocal unit (Perkin Elmer Life Sciences) and a Hamamatsu Orca-ER camera. Bright field imaging used transmission optics and an EM-CCD camera (Andor Ixon+ DU885K). Image analysis was performed in ImageJ (http://rsb.info.nih.gov/ij/).

Analysis of node motions

A single focal plane of protoplasts expressing Rlc1p-3GFP was imaged for 100–550 s at 1 s intervals. Diffusing node positions (Fig. S1C,D) were determined by Gaussian fitting. Bayesian analysis of node MSDs used the MSD-Bayes package (Monnier et al., 2012) in MATLAB. Velocities and durations of motion of nodes undergoing directed stop-go motion were determined from the constant-velocity phase of kymographs (Fig. S1F).

Analysis of formin distribution and component motions in the ring

After background subtraction, intensity was summed over the ring width. Velocities were determined from slopes of lines drawn over formin and myosin tracks in kymographs. Speed distributions were weighted by the duration and mean fluorescence intensity of each track. Formin spatial distributions were measured at the first imaging step to avoid photobleaching.

Measurement of sizes and shapes of protoplasts and contractile rings

The ImageJ Reslice function was used to view the ring face-on. From maximum intensity projections, the ring length L was measured by tracing the ring, and the protoplast circumference L_{proto} and cell deformation factor were measured by tracing the cell perimeter. Ring curvature was calculated from the radius of the best fit circle to a curve drawn over the ring viewed from above.

Measurement of contractile ring tension

See Extended Experimental Procedures for details. We measured the ring tension in protoplasts by first measuring the plasma membrane tension using micropipette aspiration, and then using a force balance at a furrow created by the ring. In brief, the aspiration pressure was increased in steps every 15–110 s and bright field images were recorded every 0.5 s. Membrane tension is given by $\sigma = \Delta P R_p/[2(1 - R_p/R_c)]$, where R_p is the pipette radius, R_c is the radius of the spherical protoplast cap, and ΔP is the suction pressure required to aspirate an equilibrium length $l = R_p$ of protoplast into the pipette.

The ring tension T was then inferred from protoplasts with sliding rings that furrowed the membrane, using the force balance $T = R_{ring}(\sigma_1 \cos\theta_1 + \sigma_2 \cos\theta_2)$, where R_{ring} is the ring radius, θ_1 and θ_2 are the angles the membrane makes with the plane of the ring at the furrow, and σ_1 and σ_2 are the membrane tensions of the two protoplast lobes. The mean of the membrane tensions of the two lobes was assumed to equal the value of the membrane tension σ that we measured as described above.

Contractile ring simulation

See Extended Experimental Procedures.

Supplementary Material

Refer to Web version on PubMed Central for supplementary material.

Acknowledgments

We thank P. Garcia for performing preliminary experiments. This work was supported by NIH grants GM086731 to B.O. and GM026132 to T.D.P. C.L. was supported by a HFSP Long-Term Fellowship. H.F.C is a Merck-LSRF Fellow.

References

Bezanilla M, Wilson JM, Pollard TD. Fission yeast myosin-II isoforms assemble into contractile rings at distinct times during mitosis. Curr Biol. 2000; 10:397–400. [PubMed: 10753748]

Biron D, Alvarez-Lacalle E, Tlusty T, Moses E. Molecular model of the contractile ring. Phys Rev Lett. 2005; 95:098102. [PubMed: 16197254]

Carvalho A, Desai A, Oegema K. Structural memory in the contractile ring makes the duration of cytokinesis independent of cell size. Cell. 2009; 137:926–937. [PubMed: 19490897]

Chen Q, Nag S, Pollard TD. Formins filter modified actin subunits during processive elongation. J Struct Biol. 2012; 177:32–39. [PubMed: 22056467]

Evans E, Yeung A. Apparent viscosity and cortical tension of blood granulocytes determined by micropipet aspiration. Biophys J. 1989; 56:151–160. [PubMed: 2752085]

Fujiwara K, Pollard TD. Fluorescent-antibody localization of myosin in cytoplasm, cleavage furrow, and mitotic spindle of human cells. J Cell Biol. 1976; 71:848–875. [PubMed: 62755]

Huxley AF. Muscular contraction. J Physiol (Lond). 1974; 243:1–43. [PubMed: 4449057]

Jochova J, Rupes I, Streiblova E. F-actin contractile rings in protoplasts of the yeast Schizosaccharomyces. Cell Biol Int Rep. 1991; 15:607–610. [PubMed: 1934083]

Kamasaki T, Osumi M, Mabuchi I. Three-dimensional arrangement of F-actin in the contractile ring of fission yeast. J Cell Biol. 2007; 178:765–771. [PubMed: 17724118]

Kanbe T, Kobayashi I, Tanaka K. Dynamics of cytoplasmic organelles in the cell cycle of the fission yeast Schizosaccharomyces pombe: 3-dimensional reconstruction from serial sections. J Cell Sci. 1989; 94:647–656. [PubMed: 2630561]

Kovar DR, Harris ES, Mahaffy R, Higgs HN, Pollard TD. Control of the assembly of ATP- and ADP-actin by formins and profilin. Cell. 2006; 124:423–435. [PubMed: 16439214]

Laporte D, Coffman VC, Lee IJ, Wu JQ. Assembly and architecture of precursor nodes during fission yeast cytokinesis. J Cell Biol. 2011; 192:1005–1021. [PubMed: 21422229]

Laporte D, Ojkic N, Vavylonis D, Wu JQ. Alpha-actinin and fimbrin cooperate with myosin II to organize actomyosin bundles during contractile ring assembly. Mol Biol Cell. 2012; 23:3094–3110. [PubMed: 22740629]

Lenz M, Thoresen T, Gardel ML, Dinner AR. Contractile units in disordered actomyosin bundles arise from f-actin buckling. Phys Rev Lett. 2012; 108

Lord M, Pollard TD. UCS protein Rng3p activates actin filament gliding by fission yeast myosin-II. J Cell Biol. 2004; 167:315–325. [PubMed: 15504913]

Mabuchi I, Okuno M. Effect of myosin antibody on division of starfish blastomeres. J Cell Biol. 1977; 74:251–263. [PubMed: 141455]

Mendes Pinto I, Rubinstein B, Kucharavy A, Unruh JR, Li R. Actin depolymerization drives actomyosin ring contraction during budding yeast cytokinesis. Dev Cell. 2012; 22:1247–1260. [PubMed: 22698284]

Michelot A, Berro J, Guerin C, Boujemaa-Paterski R, Staiger CJ, Martiel JL, Blanchoin L. Actin-filament stochastic dynamics mediated by ADF/cofilin. Curr Biol. 2007; 17:825–833. [PubMed: 17493813]

Mishra M, Huang YY, Srivastava P, Srinivasan R, Sevugan M, Shlomovitz R, Gov N, Rao M, Balasubramanian M. Cylindrical cellular geometry ensures fidelity of division site placement in fission yeast. J Cell Sci. 2012; 125:3850–3857. [PubMed: 22505610]

Mishra M, Kashiwazaki J, Takagi T, Srinivasan R, Huang Y, Balasubramanian MK, Mabuchi I. In vitro contraction of cytokinetic ring depends on myosin II but not on actin dynamics. Nat Cell Biol. 2013; 15:853–859. [PubMed: 23770677]

Monnier N, Guo SM, Mori M, He J, Lenart P, Bathe M. Bayesian approach to msd-based analysis of particle motion in live cells. Biophys J. 2012; 103:616–626. [PubMed: 22947879]

Naqvi NI, Eng K, Gould KL, Balasubramanian MK. Evidence for F-actin-dependent and -independent mechanisms involved in assembly and stability of the medial actomyosin ring in fission yeast. EMBO J. 1999; 18:854–862. [PubMed: 10022828]

Pelham RJ, Chang F. Actin dynamics in the contractile ring during cytokinesis in fission yeast. Nature. 2002; 419:82–86. [PubMed: 12214236]

Pollard TD, Wu JQ. Understanding cytokinesis: Lessons from fission yeast. Nat Rev Mol Cell Biol. 2010; 11:149–155. [PubMed: 20094054]

Rappaport R. Cell division: Direct measurement of maximum tension exerted by furrow of echinoderm eggs. Science. 1967; 156:1241–1243. [PubMed: 6067406]

Rappaport R. Tensiometric studies of cytokinesis in cleaving sand dollar eggs. Journal of Experimental Zoology. 1977; 201:375–378. [PubMed: 561826]

Schroeder TE. The contractile ring. II Determining its brief existence, volumetric changes, and vital role in cleaving arbacia eggs. J Cell Biol. 1972; 53:419–434. [PubMed: 5063470]

Schroeder, TE. Dynamics of the contractile ring In Molecules and cell movement. Inoue, S.; Stephens, RE., editors. New York: Raven Press; 1975. p. 305-332.

Schroeder TE, Otto JJ. Immunofluorescent analysis of actin and myosin in isolated contractile rings of sea-urchin eggs. Zool Sci. 1988; 5:713–725.

Sipiczki M, Bozsik A. The use of morphomutants to investigate septum formation and cell separation in Schizosaccharomyces pombe. Arch Microbiol. 2000; 174:386–392. [PubMed: 11195093]

Vavylonis D, Wu JQ, Hao S, O'Shaughnessy B, Pollard TD. Assembly mechanism of the contractile ring for cytokinesis by fission yeast. Science. 2008; 319:97–100. [PubMed: 18079366]

Wloka C, Vallen EA, The L, Fang X, Oh Y, Bi E. Immobile myosin-II plays a scaffolding role during cytokinesis in budding yeast. J Cell Biol. 2013; 200:271–286. [PubMed: 23358243]

Wu JQ, Bahler J, Pringle JR. Roles of a fimbrin and an alpha-actinin-like protein in fission yeast cell polarization and cytokinesis. Mol Biol Cell. 2001; 12:1061–1077. [PubMed: 11294907]

Wu JQ, Pollard TD. Counting cytokinesis proteins globally and locally in fission yeast. Science. 2005; 310:310–314. [PubMed: 16224022]

Yonetani A, Lustig RJ, Moseley JB, Takeda T, Goode BL, Chang F. Regulation and targeting of the fission yeast formin cdc12p in cytokinesis. Mol Biol Cell. 2008; 19:2208–2219. [PubMed: 18305104]

Zhang WD, Robinson DN. Balance of actively generated contractile and resistive forces controls cytokinesis dynamics. Proc Natl Acad Sci USA. 2005; 102:7186–7191. [PubMed: 15870188]

Zumdieck A, Kruse K, Bringmann H, Hyman AA, Julicher F. Stress generation and filament turnover during actin ring constriction. PLoS ONE. 2007; 2:e696. [PubMed: 17684545]

HIGHLIGHTS

1. Observations of live protoplasts provided information to model the contractile ring
2. Computer simulations produced a self-organizing, tension-generating actomyosin ring
3. Turnover and self-organization of proteins continuously remodel a constricting ring
4. Constricting ring shapes show that rings set the tension, not the constriction rate

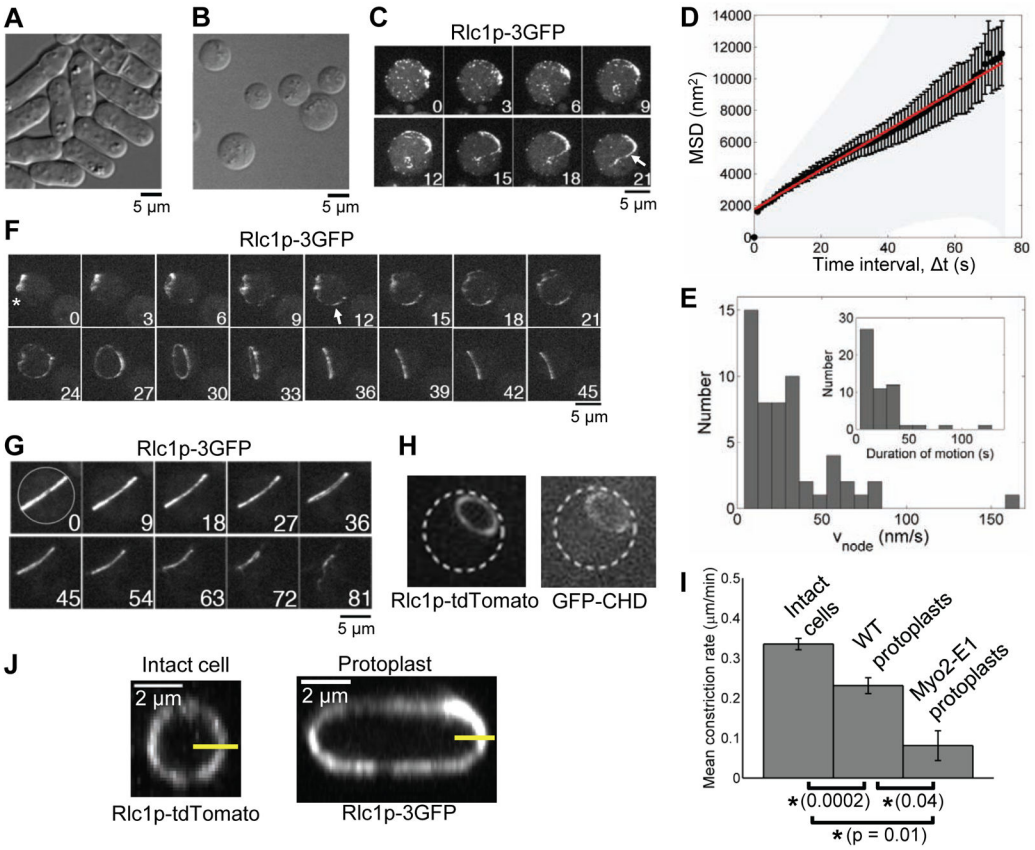

Figure 1. Formation and constriction of contractile rings in fission yeast protoplasts

(A and B) Differential interference contrast (DIC) micrographs of (A) intact fission yeast cells and (B) protoplasts.

(C, F and G) Time series of fluorescence micrographs of protoplasts expressing Rlc1p-3GFP. These projections were assembled from Z-stacks of confocal images acquired at intervals indicated in min.

(C) Nodes marked with Rlc1p-3GFP coalesce into a strand (arrow).

(D) Node diffusion in protoplasts. Graph of average mean square displacement (filled circles, n = 64 nodes in 15 cells) ±SEM (error bars) and ±SD (light gray area). Red line: best fit straight line to average MSD. See also Movie S1.

(E) Directed motions of nodes in protoplasts. Distributions of speeds and (inset) durations of motions. See also Movie S2.

(F) Assembly of a contractile ring from a strand (arrow) originating from a disassembling ring (asterisk).

(G)Constriction of a contractile ring by sliding along the plasma membrane. See also Movie S3.

(H) Epifluorescence images of a protoplast (outlined with white dashes) expressing myosin light chain Rlc1p-tdTomato and GFP-Rng2p calponin homology domain (GFP-CHD) to label actin filaments. The ring contains both myosin-II and actin filaments.

(I) Comparison of ring constriction rates in intact cells (n = 20), wild-type protoplasts (n = 18) and *myo2-E1* mutant protoplasts (n = 3, mean ± SEM). Asterisks, $p < 0.05$; ns, not significant.

(J) Images in the plane of contractile rings from 3D reconstructions of stacks of fluorescence micrographs of (left) an intact cell and (right) a protoplast expressing tagged myosin-II, used to measure the ring thickness perpendicular to the plasma membrane (yellow lines). See also Fig. S3A,B.

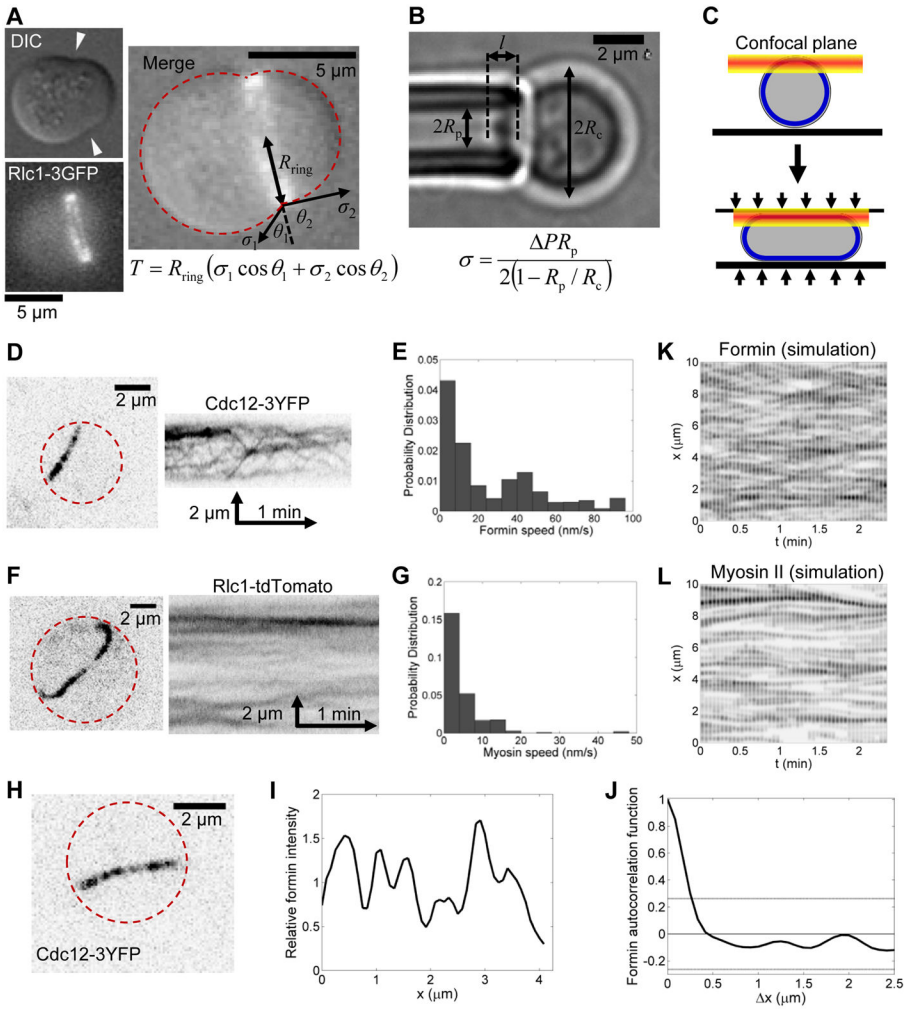

Figure 2. Contractile ring tension, component organization and component motions

Dashedred lin es show cell boundaries.

(A) DIC and fluorescence micrographs of a protoplast expressing Rlc1p-3GFP and deformed by the constricting contractile ring (arrowheads). The merged image is labeled with the quantities used to measure ring tension *T* from a force balance with membrane tension.

(B) Bright field image of a protoplast undergoing micropipette aspiration to measure membrane tension σ. Pressure Δ*P*= 873 Pa. See also Fig. S2H.

(C) Schematic showing protoplast compression to image long spans of contractile rings in a single confocal plane.

(D and F) Reverse-contrast confocal fluorescence (left) images and (right) kymographs of compressed protoplasts expressing (D) formin Cdc12p-3YFP or(F) Rlc1p -tdTomato to mark myosin-II.

(E and G) Distributions of the speeds of fluorescent spots in contractile rings. (E) Spots of Cdc12p-3YFP (n = 17 rings) move faster than (G) spots of Rlc1p-tdTomato (n = 4 rings). See also Movies S4 and S5.

(H) Reverse-contrast confocal fluorescence image of a segment of a contractile ring on one flattened surface of a compressed protoplastexpressing Cdc12p-3YFP.
(I) Fluorescence intensity profile along the ring in (H). Mean intensity is defined to be 1.
(J) The mean spatial autocorrelation function of formin Cdc12p-3YFP intensity (n = 17 rings) decays rapidly to values not significantly different from zero, showing that the fluorescence is randomly distributed around the ring. Dashed gray lines: mean 95% confidence intervals.
(K and L) Kymographs showing motions of (K) formin and (L) myosin in the ring simulation.
Reverse contrast images were convolved with a point spread function (standard deviation 0.1 μm) for comparison with the experiments of D and F.

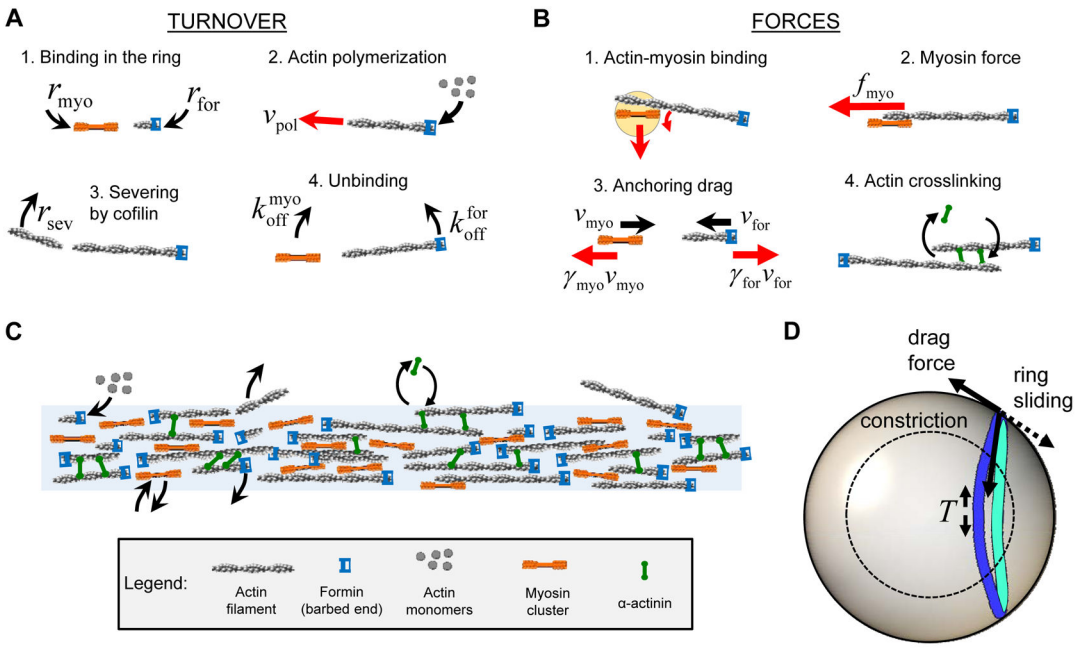

Figure 3. Stochastic simulation of the fission yeast contractile ring

(A) Turnover reactions. Formin (blue) and myosin-II clusters (orange) bind the plasma membrane at random locations around the ring and subsequently unbind (Table S1). Formins nucleate actin filaments (gray) that polymerize at rate v_{pol} in random directions, and are severed by cofilin at rate r_{sev} per filament length.

(B) Forces in the simulation. Myosin-II clusters bind actin filaments within the capture radius (light orange), and pull them to generate tension. Drag forces on membrane anchors resist formin and myosin-II motions (drag coefficients γ_{for}, γ_{myo}). Dynamic α-actinin crosslinks bundle neighboring actin filaments.

(C) Schematic illustration of the self-organized ring, a dynamic bundle of crosslinked actin filaments tensed by myosin-II clusters.

(D) Sliding-constriction model of rings in protoplasts. The ring tension T, calculated from the ring simulation (panels A–C), is input to this model. Anchor drag forces bend the ring out of plane.

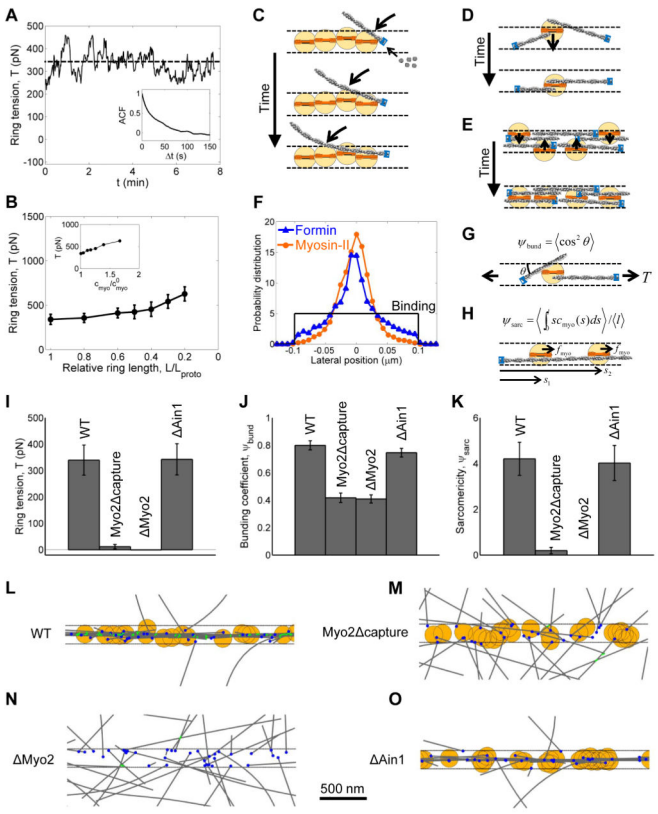

Figure 4. Simulations produce self-organized contractile rings that generate tension

(A) Time course of tension (solid line) in a simulated contractile ring. The mean tension (dashed line) was 340 pN at the onset of constriction ($L = L_{proto}$). Fluctuations reflect continuous renewal of ring organization. (Inset) tension autocorrelation function (memory time 29.4 s, exponential fit).

(B) Mean tensions in simulated rings of different lengths. Tension increases as the ring constricts due to increasing myosin-II concentration (Inset and Fig. S1H).

(C–E) Schematics of three factors driving ring self-organization: (C) sequential binding and zippering of actin filaments by myosin-II; (D) filament alignment due to myosin-II mobility; and (E) condensation of myosin into the midline of the ring.

(F) Myosin and formin distributions across the width of the simulated ring. (Black) Binding occurs uniformly in a zone 0.2 μm wide. (Blue and orange) At steady state, myosin and formin concentrate into a band ~70nm wide at the midline of the ring (n = 8 simulated rings, 10 μm long).

(G and H) Ring tension depends on ring organization through (G) the bundling coefficient, Ψ_{bund}, measuring the alignment of tensile actin filaments along the ring, and (H) the sarcomericity, Ψ_{sarc}, measuring the number of actin-myosin interactions weighted by their locations relative to actin barbed ends.

(I–O) Simulations to test contributions of myosin-II and α-actinin to ring self-organization and tension. WT: wild type (full model). Myo2Δcapture: myosin clusters pull actin filaments toward the pointed end, but cannot capture and thereby rotate filaments. ΔMyo2: no myosin-II. ΔAin1: no α-actinin.

(I–K) Capture of actin filaments by myosin-II clusters is required for (I) ring tension, (J) filament bundling and (K) sarcomericity.

(L–O) Images of steady state rings simulated under the four conditions. See Movie S6 for the wild type simulation. (L) Actin and myosin-II self-organize into a tightly bundled ring. (M and N) Myosin-II that can capture actin filaments is required to organize a ring, but (O) not α-actinin.

Color code: gray, actin filaments; orange, myosin capture zone; blue, formins; green, α-actinin crosslinks. Horizontal lines: boundaries of formin and myosin binding zone.

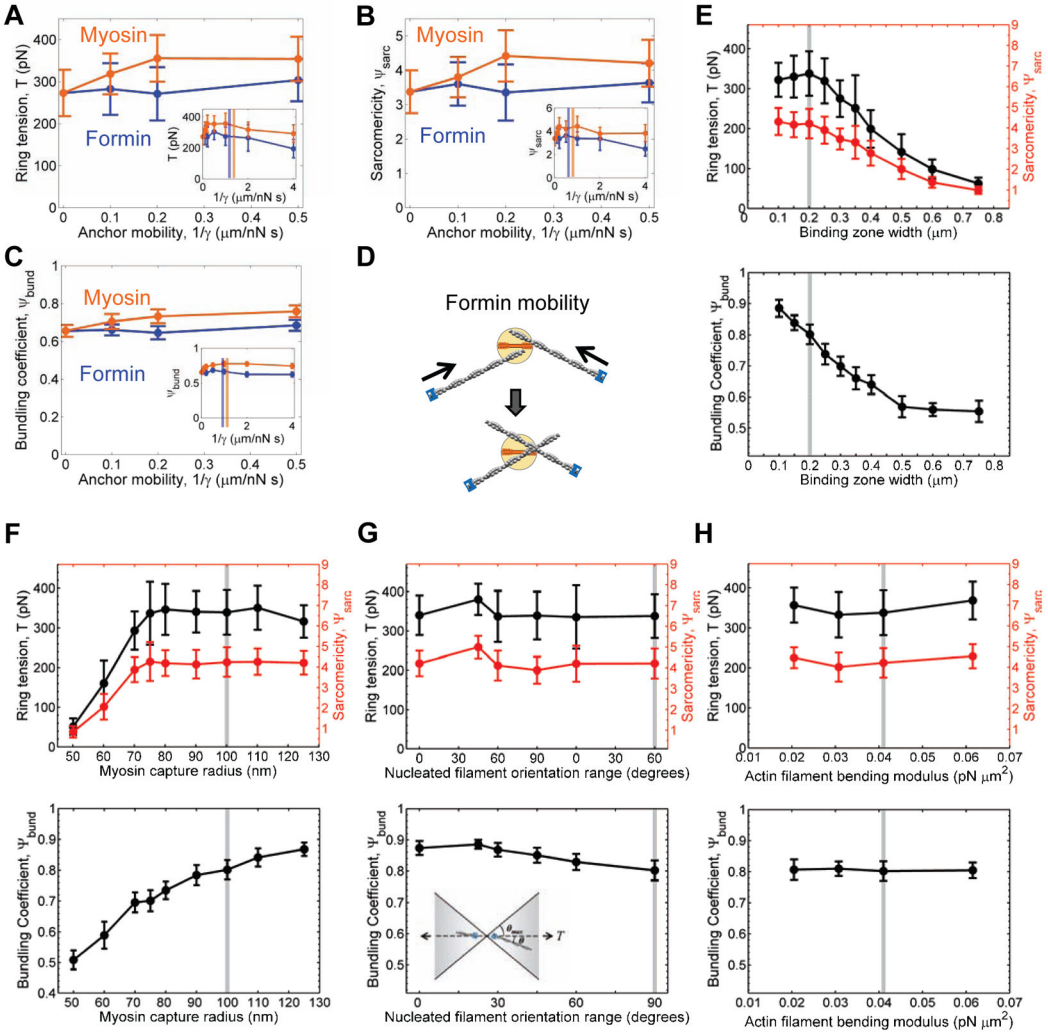

Figure 5. Tension and organization in simulated rings is robust with respect to model parameters

(A–C) Effects of the mobility of (orange) myosin and (blue) formin anchors on simulated (A) ring tension, (B) sarcomericity and (C) bundling coefficient. For each case, the other component was immobilized. Vertical lines: best fit values.

(D) By allowing actin filaments to be pulled toward the myosin, increasing formin mobility causes decay of sarcomericity and tension.

(E–H) Sensitivity of simulated ring tension (top, black), sarcomericity (top, red) and bundling coefficient (bottom) on model parameter values: width of the binding zone for formin and myosin-II (E); myosin cluster capture radius for binding to actin filaments (F); range of orientations (inset) of actin filaments randomlynucleated by formins (G); actin filament bending modulus (H). Grey line: standard parameter values (wild-type simulations, Table S1). Error bars indicate S.D.

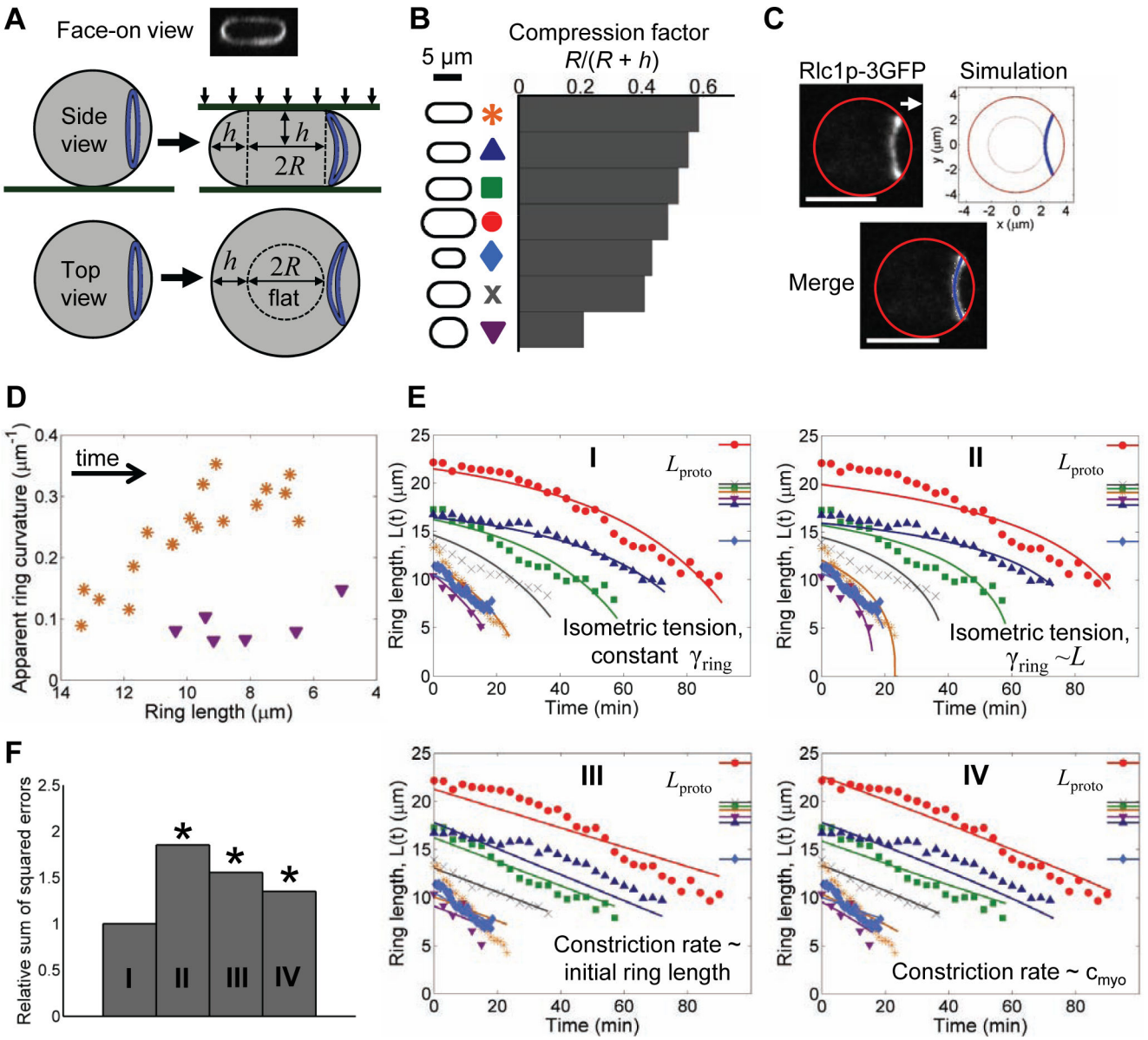

Figure 6. Sliding-constriction model reproduces observed ring shapes and constriction rates in protoplasts

(A) Schematic of protoplasts compressed with coverslips showing the definition of the radius *R* and half-height *h* of the flat portion. Top: Face-on view of a ring in a compressed protoplast expressing Rlc1p-3GFP, reconstructed from a Z-series of confocal fluorescence micrographs.

(B) Silhouettes of 7 protoplasts compressed into different cheese wheel shapes characterized by the compression factor. These cells were used to study ring shapes and constriction rates in panels C–E.

(C) Comparison of the observed and predicted shape of a constricting ring in a compressed protoplast (*h* = 1.6 µm, *R* = 2.3 µm), viewed from above. (Left) Maximum projection of confocal sections of Rlc1p-3GFP fluorescence. (Right) Ring shape predicted by the sliding-

constriction model, blue. (Bottom) Merge. The ring bends out of plane. Solid and dotted red lines show, respectively, boundaries of the cell and the flat portion of the cell. Bar: 5 μm. See also Fig. S4A and Movie S7.

(D) Measured curvature of rings (viewed from above) from the most and least flattened cells. Curvature increases with ring constriction and is greater in the more compressed protoplast, in agreement with model. Symbols as in (B). See also Fig. S4B.

(E) Time course of the length of rings constricting in the 7 cells of (B). Least squares fits (solid lines) of four candidate models (I–IV) to experimental data (discrete markers). (I) Sliding-constriction model with constant ring-membrane drag coefficient γ_{ring}; (II) sliding-constriction model with γ_{ring} proportional to ring length; (III) model with a constant constriction rate proportional to initial ring length; (IV) model with a constriction rate proportional to myosin concentration. Symbols at right show protoplast equatorial circumferences. See Fig. S4C for additional cells included in the fits (n = 17 total).

(F) Residual sum of squares for model fits from (E) and Fig. S4C, normalized by the model I value. Asterisks indicate a poor fit ($p<10^{-5}$, chi-squared test). Variance in $L(t)$ due to measurement error was assumed to be the variance of model errors from model I.

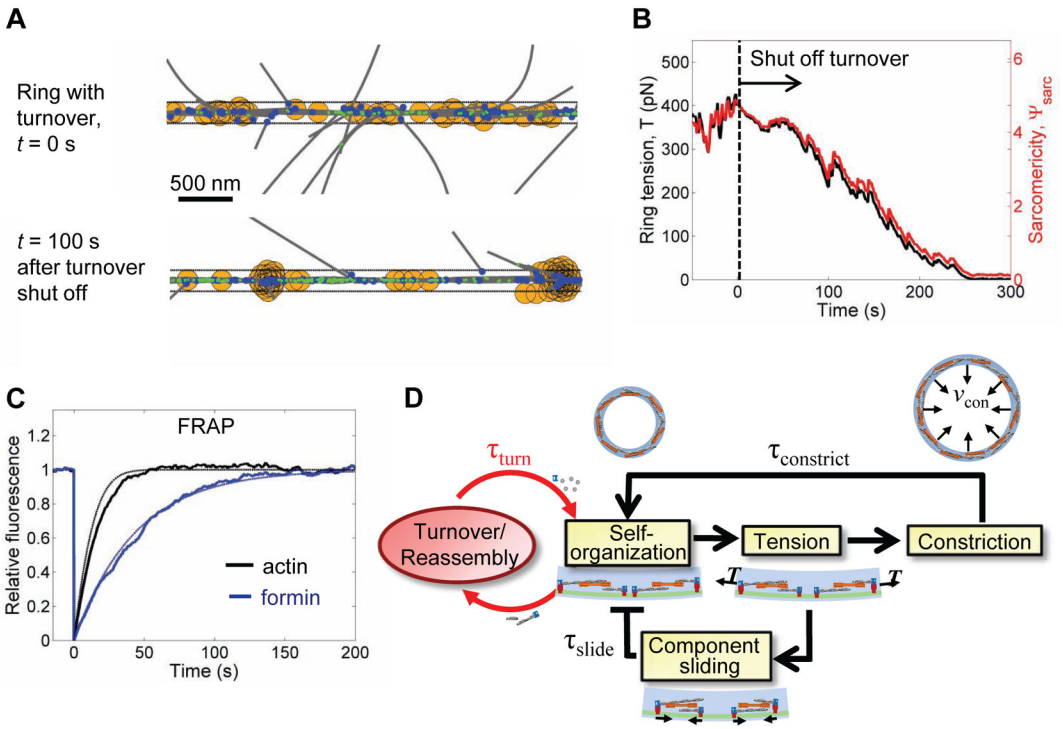

Figure 7. Turnover and self-organization maintain ring tension and remodel the constricting ring

(A) Time-lapse images of a simulated ring. (Top) Ring at steady state. (Bottom) Same ring 100 s after switching off formin, actin, and myosin-II turnover. Color code: gray, actin filaments; orange, myosin capture zone; blue, formins; green, α-actinin crosslinks.

(B) Ring tension and sarcomericity decay after switching off turnover at time $t = 0$.

(C) Simulations (thick lines, mean of 10 simulations), and exact solutions (thin lines, see Supplemental Experimental Procedures) for FRAP assays of steady state contractile rings. (Black) Actin is predicted to recover in $t_{1/2} = 11$ s. (Blue) By comparison, formin recovered in $t_{1/2} = 30$ s (blue), determined by fitting to experimental FRAP data (Fig. S3C).

(D) Remodeling mechanisms that emerge from the ring simulations. In protoplasts tension drives constriction, but also circumferential sliding of membrane-anchored components that would decay organization and tension after time τ_{slide}. Rapid turnover and self-organization continuously reassemble the ring, preventing the decay ($\tau_{turn} \ll \tau_{slide}$), and gradually remodeling the ring as it constricts ($\tau_{turn} \ll \tau_{constrict}$).